catalysts

MDPI

Article

Photocatalytic NO_x Removal in Bismuth-Oxyhalide (BiOX, X = I, Cl) Cement-Based Materials Exposed to Outdoor Conditions

Magaly Y. Nava-Núñez [1], Eva Jimenez-Relinque [2], Azael Martínez-de la Cruz [1] and Marta Castellote [2,*]

[1] CIIDIT, Facultad de Ingeniería Mecánica y Eléctrica, Universidad Autónoma de Nuevo León, Ciudad Universitaria, San Nicolás de los Garza 66451, Mexico
[2] Eduardo Torroja Institute of Construction Sciences, IETcc, CSIC, Serrano Galvache 4, 28033 Madrid, Spain
* Correspondence: martaca@ietcc.csic.es

Abstract: Cement-based materials modified with 3D BiOX (X = I, Cl) microspheres at different percentages (1, 5 and 10% by weight of the cement binder) were prepared to investigate the durability of the photocatalytic NO_x removal under outdoor conditions. Weathering—corresponding to a period of 13 months outdoors—was studied in terms of NO removal efficiency under visible and UVA light irradiation for BiOI and BiOCl mortars, respectively. Following this period, the samples were protected from the environment for four years, and NO_x removal and selectivity to nitrates were assessed. BiOI and BiOCl mortar samples were initially photocatalytically active; NO_x removal performance increased as BiOX content increased. There was good photocatalyst dispersion, and compressive strength was not significantly impacted. The BiOI mortars had nearly completely lost their activity after 5 years from casting, whereas mortars containing 10% BiOCl had maintained about 7% of initial performance. The results suggest that mortar deactivation is due to surface dirt and nitrates accumulation from NO_x oxidation on the surface rather than carbonation. An internal self-deactivation mechanism that affects BiOI in mortar matrix has also been postulated.

Keywords: BiOX; photocatalysis; mortar; NO_x; outdoor exposure; self-deactivation

Citation: Nava-Núñez, M.Y.; Jimenez-Relinque, E.; Martínez-de la Cruz, A.; Castellote, M. Photocatalytic NO_x Removal in Bismuth-Oxyhalide (BiOX, X = I, Cl) Cement-Based Materials Exposed to Outdoor Conditions. *Catalysts* **2022**, *12*, 982. https://doi.org/10.3390/catal12090982

Academic Editors: Yu Huang and Qian Zhang

Received: 28 July 2022
Accepted: 26 August 2022
Published: 31 August 2022

1. Introduction

Recent environmental regulations have stimulated the development of new constructive strategies and smart materials intended to reduce the human health effects of poor air quality in urban areas. This focus resulted in significant growth in the research of construction materials containing photocatalysts to reduce environmental pollution [1–8]. So far, various classes of pavement materials functionalized with photocatalytic nanoparticles have been developed and tested on both laboratory and pilot scales [9–13]. Both indoor and outdoor building environments are exposed to chemical contamination from internal sources (furniture, paint, heaters, appliances, etc.) and external sources (traffic and industry), resulting in the presence of various pollutants (VOC, NO_x, SO_x, formaldehyde, PMs, CO, etc.) [14–17]. With respect to pollutants from external sources, NO_x is common in urban areas, contributing to the formation of acid rain and photochemical smog, and it is linked to a variety of chronic respiratory disorders as heart disease, asthma and lung cancer [18].

In the field of photocatalytic construction and building materials, nanosized titanium dioxide (TiO_2) is the most widely used photocatalyst because of its compatibility with conventional building materials and its excellent photocatalytic properties. TiO_2-containing construction materials can be obtained by mixing or coating techniques (e.g., dip-coating, spin-coating, spraying, or brushing) using various rigid substrates, such as cement [19–22], paints [15,23–25], stucco [26], tiles [15,27,28] and glass [29]. Among them, cement-based

materials (pastes, mortars and concretes) are the most commonly used building materials in the construction industry.

The main barrier to large-scale TiO_2 implementation is its wide bandgap (~3.2 eV for anatase and ~3.0 eV for rutile), which limits its adsorption to UV light (about 5% of the overall solar spectrum). Another significant drawback of TiO_2 is its high photogenerated electron-hole recombination, which reduces overall reaction efficiency [30–32]. Furthermore, the use of nanoparticles continues to spark debate about the impact of their inhalation on human health [33,34]. The European Union has typified exposure to nanoparticles as one of the emerging risks, and the Committee for Risk Assessment proposed to classify respirable TiO_2 as carcinogen category 2: inhalation of mixtures in powder form containing 1% or more of TiO_2, which is in the form of or incorporated in particles with aerodynamic diameters $\leq$10 μm [35]. Trying to overcome these limitations, recent studies have focused on the development of alternative photocatalysts that combine a visible-light-driven response and micrometric particle size. Bismuth oxyhalides, BiOX (X = Cl, Br and I), have emerged as potential candidates for photocatalytic applications among these alternative photocatalysts. BiOX consists of $[Bi_2O_2]^{2+}$ sheets and enclosed double-layered halide ions bonded through van der Waals interactions. This structure forms an induced dipole when exposed to light, resulting in an effective separation of photogenerated electron-hole pairs. Additionally, BiOX's 3D hierarchical microstructure improves light-harvesting, shortens diffusion pathways, accelerates interfacial charge separation and creates more reactive sites, all of which enhance photocatalytic efficiencies [36–38]. Among BiOX, BiOI owns the narrowest bandgap (Eg ~ 1.8 eV), resulting in a wider response range for visible light. BiOCl can utilize the photons at wavelength shorter than 380 nm, similarly to TiO_2 (P25) [39].

There has been some progress in the application of BiOX to cement-based materials. Geng et al. [40] prepared cement pastes with a BiOBr precursor that can remove NO_x via visible light (λ > 420 nm). Similarly, Wang et al. [41] prepared BiOBr and BiOBr/SiO_2 cement composites with air purifying properties for propylene degradation under xenon lamp irradiation. Likewise, our research group has developed an inexpensive microwave-assisted solvothermal synthesis for BiOX microspheres (BiOI and BiOCl) [36]. These BiOX photocatalysts were used to prepare photocatalytic mortars that, in the case of BiOI, had better visible-light-driven NO_x removal capability than TiO_2-modified cement. A phase transformation in alkaline media was found in BiOI-cem to an I-deficient bismuth oxide compound with poor visible light absorbance capability. However, BiOI-cem showed considerably higher nitrate selectivity that resulted in the highest NO_x global removal efficiency [42].

In the present work, the performances under long-term conditions of BiOX and cement-based materials have been evaluated. BiOX and cement samples (BiOX ranging from 0% to 10% by weight) were cast, and for the first time, the real weathering effect (13 months exposure to an outdoor environment, and 4 years preserved from external agents) on the NO_x photocatalysis is given.

2. Results and Discussion

2.1. Characterization of BiOX Photocatalysts

Figure 1 shows the XPS high-resolution spectra of the BiOI sample. First, it can be seen that no other components different from Bi, O and I were detected. The high-resolution of Bi 4f spectrum showed two peaks with binding energies of 159.1 and 164.4 eV corresponding to $4f_{7/2}$ and $4f_{5/2}$, which confirmed that the bismuth species were in the BiOI in the form of Bi^{3+}. Meanwhile, the two strong peaks observed in the high-resolution XPS spectrum of I located at 630.4 and 618.8 eV were assigned to the binding energies of I $3d_{3/2}$ and I $3d_{5/2}$, respectively, confirming the existence of I^- in BiOI sample. Finally, the O1s peak observed at about 529.9 eV belonged to the bismuth–oxygen bond in BiOI. Therefore, the purity of the synthetized BIOI sample was confirmed. Similarly, in Figure 2, the BiOCl sample shows Bi $4f_{7/2}$ and $4f_{5/2}$ peak binding energies at about 159.1 and 164.5 eV, which confirmed the +3 oxidation state of bismuth. In addition, the XPS peaks of Cl 2p located at

197.9 and 199.3 eV, assigned to Cl $2p_{3/2}$ and Cl $2p_{1/2}$, certified the existence of Cl^-. Finally, the main binding energy of O 1s detected at about 530 eV corresponds to the lattice oxygen of the bismuth-oxygen bond in the BiOCl photocatalyst. These results match well with the XRD results of BiOI (standard card number 73-2062) and BiOCl (standard card number 82-0485) tetragonal phases described in [42].

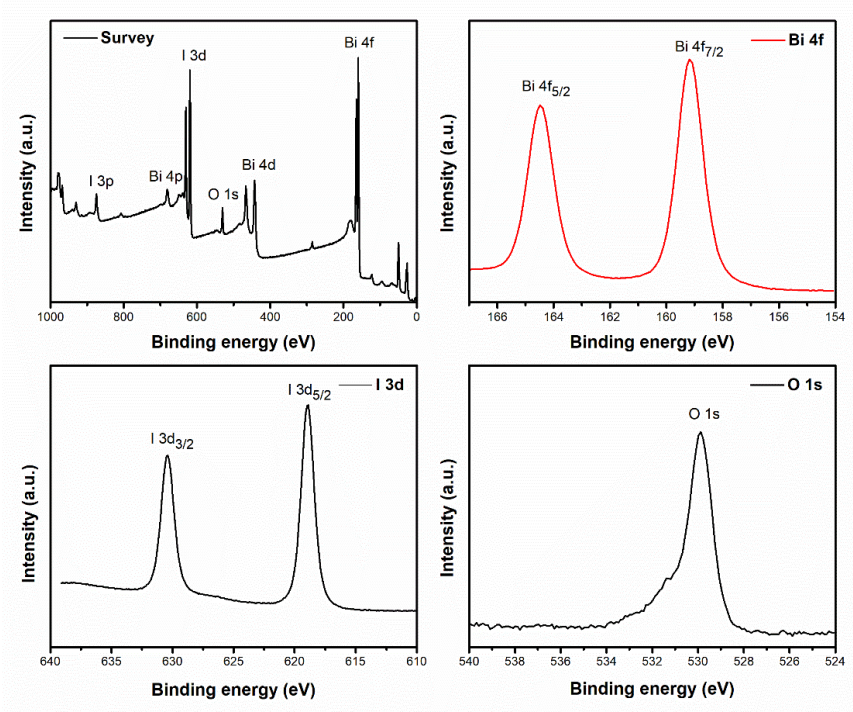

Figure 1. XPS spectra of BiOI photocatalyst.

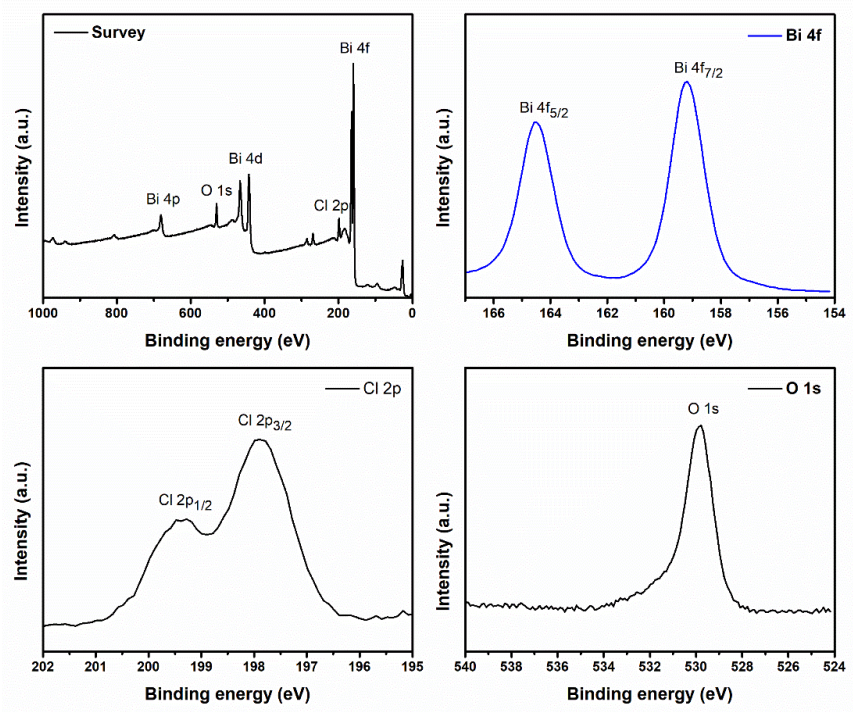

Figure 2. XPS spectra of BiOCl photocatalyst.

SEM images revealed that both BiOX photocatalysts showed 3D spherical flower-like morphology, as is shown in Figures 3 and 4. The average size of the microspheres of

BiOI varied from 1 to 1.5 µm. The high-magnification SEM image illustrated in Figure 3b revealed that these microspheres were formed by self-assembling individual 2D plate-like sheets with a thickness of about 5 nm. TEM characterization provided further insight into the interior 2D sheets structure. The high-magnification TEM image presented in Figure 3c reveals that the nanosheets were packed with a large quantity of small spherical nanocrystals that were closely interconnected with each other. According to the size distribution histogram of BiOI presented in Figure 3d, the mean crystal size was about 5 nm.

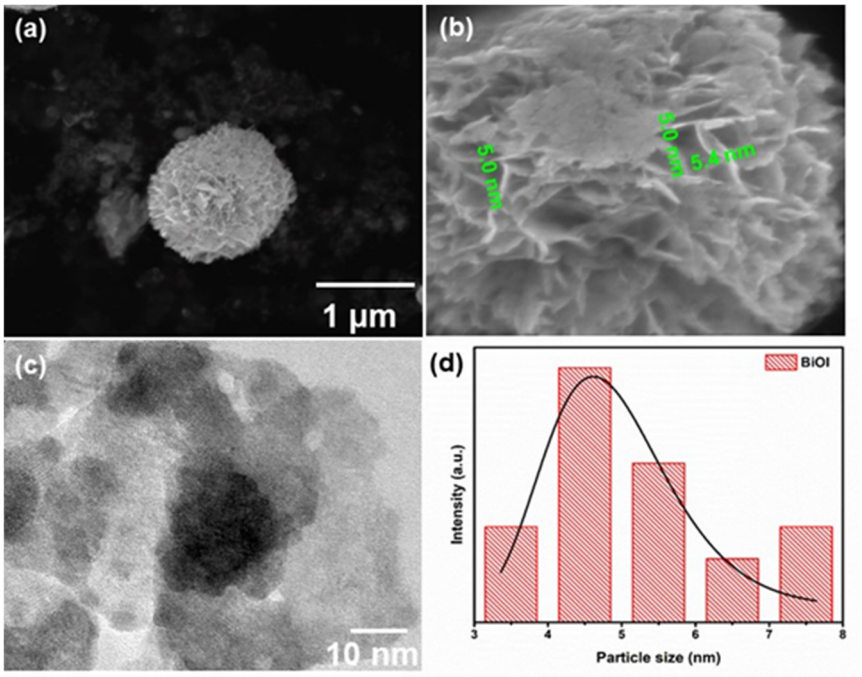

Figure 3. SEM (**a**,**b**) and TEM (**c**) images and distribution of particle size (**d**) of BiOI photocatalyst.

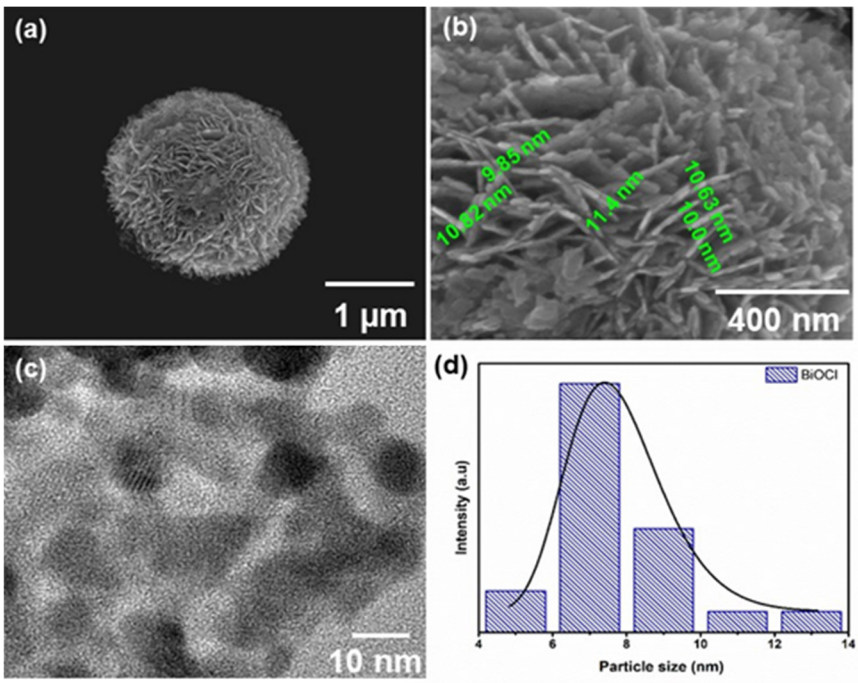

Figure 4. SEM (**a**,**b**) and TEM (**c**) images and distribution of particle size (**d**) of BiOCl photocatalyst.

The particle size of the BiOCl sample was slightly bigger compared to that of the BiOI sample. As can be seen in Figure 4a, the BiOCl microspheres were 2 to 2.5 µm across, approximately. Likewise, BiOCl microspheres were composed of a 2D plate-like sheet structure. The thickness of the nanosheets was from 9 to 11 nm, as shown in Figure 4b, thicker than the BiOI sheets. Similarly, the detailed image of BiOCl acquired by TEM, presented in Figure 4c, exhibits that nanosheets were composed of tiny nanocrystals. In this case, according to the size distribution histogram, the main size of the nanocrystal was approximate 8 nm, as it can be appreciated in Figure 4d. These results are consistent with the value of crystal size calculated from analysis X-ray peak width using the Scherrer equation (see Table 1) [42].

Table 1. Physicochemical properties of photocatalysts.

Sample	Crystallite Size (nm) [a]	Band Gap (eV) [b]	Surface Area ($m^2.g^{-1}$) [c]
BiOI	8 ± 3	1.9	57
BiOCl	12 ± 4	3.4	40
TiO_2	35 *	3.2	50

[a] Estimated from XRD by Scherrer equation (* data reported by [26]). [b] Calculated from UV-Vis absorption spectra. [c] Specific surface area estimated from BET surface area analysis (deviation ±0.01 m^2/g).

2.2. Characterization of Photocatalytic Mortar Samples

Figure 5 presents the compressive strength levels of the reference and photocatalytic mortars at 10% wt. at the age of 28 days. The addition of BiOX photocatalysts had no effect on the compressive strength when compared to the reference mortar. All the samples presented similar values of compressive strength between 42.6 and 43.4 Mpa.

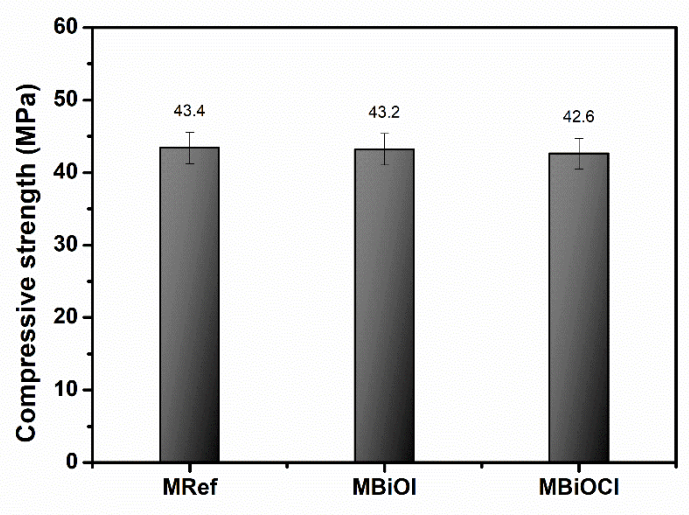

Figure 5. Compressive strength properties of reference (MRef) and photocatalytic mortars prepared with 10% of the photocatalyst (BiOI or BiOCl) at the age of 28 days.

Figure 6a shows the XRD patterns of reference (MRef) and photocatalytic mortar prepared with BiOI (MBiOI-10). Both mortar samples presented the main hydration products of ordinary Portland cement as hydrated calcium silicates (CSH gels) and portlandite (calcium hydroxide, CH) together with silica in quartz form. Minor amounts of alite (tricalcium silicate, C_3S) and belite (dicalcium silicate C_2S) were also detected in the mortar samples. MBiOI-10 samples showed the diffraction peaks of pure BiOI photocatalyst; however, the position of the diffraction line corresponding to the (110) crystal plane was modified. This behavior was reported in our previous study and was associated with the phase transformation from BiOI to I-deficient bismuth oxyiodide phases as Bi_2O_3 and Bi_5O_7I due to alkaline pH conditions of cementitious matrix [42]. The XRD pattern of the BiOCl photocatalyst

(Figure 6b) revealed the diffraction peaks at 2θ = 25.90° and 32.55° belonging to the (101) and (110) crystal planes of tetragonal BiOCl. No other peaks were detected in MBiOCl-10, which indicated that the crystalline structure of BiOCl photocatalyst was not affected by the incorporation into cementitious materials.

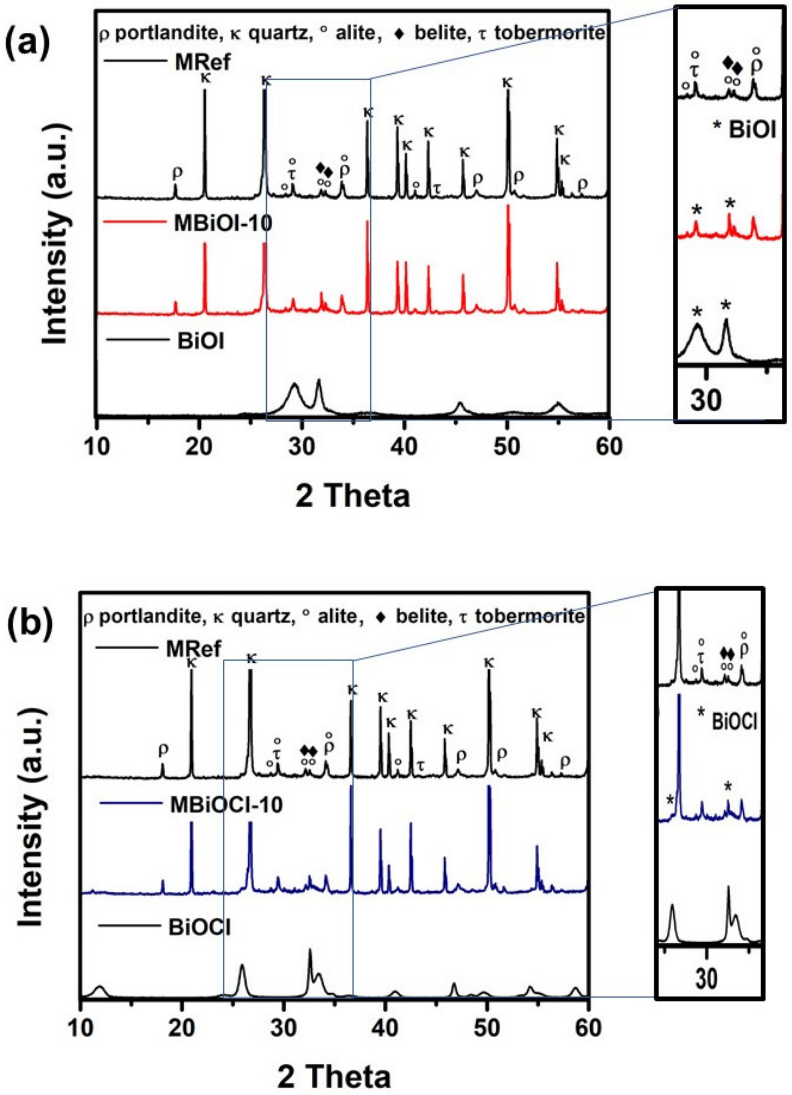

Figure 6. Comparative of XRD patterns of reference (MRef) and photocatalytic mortars: (**a**) MBiOI-10 and (**b**) MBiOCl-10. BiOCl and BiOI are XRD patterns of photocatalysts alone.

Figure 7 illustrates the SEM image with the corresponding EDS analysis of the MBiOI-10 sample. It displayed a dense microstructure; the CSH gel was the most abundant phase present on the matrix of the mortar. A small number of hexagonal portlandite crystals and thin needle-like ettringite indicated a normal hydration process (Figure 7a). A higher magnification image confirmed the presence of 3D microspheres of BiOI photocatalyst (Figure 7b). BiOI photocatalyst was well distributed in all the matrix of the mortar, and no agglomeration of particles was observed. A homogeneous dispersion of photocatalyst in the cementitious matrix is important to ensure an effective surface area, which could contribute to maximizing the photocatalytic potential to remove the pollutants [43]. The EDS analysis of MBiOI-10 sample (Figure 7c,d) confirmed that the compositions of the samples were typical of Portland cement paste; the presence of Bi and I correspond to the BiOI photocatalyst.

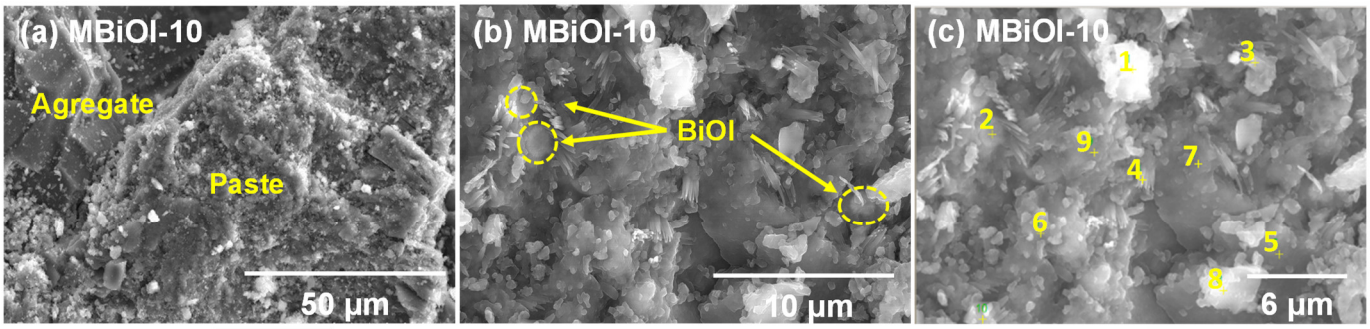

(d) MBiOI-10

Point	I	Bi	SiO_2	Al_2O_3	MgO	Fe_2O_3	CaO	SO_3	Weight (%)
1	0.52	4.83	26.33	15.52	4.29	9.85	34.86	1.89	98.09
2	6.15	44.96	5.77	0.14	0.00	0.00	42.29	0.69	100.00
3	1.28	5.12	13.43	2.62	0.00	2.32	71.04	4.17	99.98
4	1.87	5.69	12.46	1.12	0.00	1.70	74.70	2.38	99.92
5	2.21	14.83	20.86	1.30	0.00	1.47	57.66	1.64	99.97
6	2.08	7.99	13.71	1.83	0.00	0.34	70.08	3.95	99.98
7	2.03	8.57	14.35	1.63	0.00	1.49	69.31	2.59	99.97
8	1.00	1.59	71.24	1.79	1.30	0.32	20.86	1.43	99.53
9	1.74	9.49	10.23	0.88	0.00	2.00	72.33	3.30	99.97

Figure 7. SEM images (**a**–**c**) and EDS microanalysis (**d**) of MBIOI-10 mortar at 28 days.

Figure 8a,b shows that the particles of the BiOCl photocatalyst were slightly wrapped by the solid hydration products, making it more difficult to identify them. However, the elements Bi and Cl could be identified by EDS, confirming the presence of BiOCl on the photocatalytic mortar's surface.

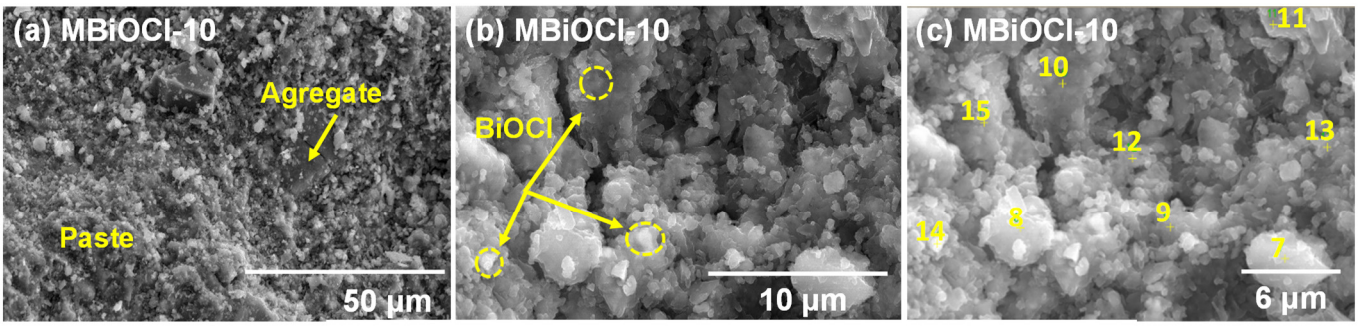

(d) MBiOCl-10

Point	Cl	Bi	SiO_2	Al_2O_3	MgO	Fe_2O_3	CaO	SO_3	Weight (%)
7	1.99	0.51	21.53	5.80	2.53	1.30	59.12	6.12	98.90
8	1.49	3.20	17.50	17.47	2.27	1.72	50.26	5.27	99.18
9	1.64	5.02	14.26	6.58	2.02	2.64	61.41	5.20	98.77
10	2.22	18.83	13.03	3.61	0.00	0.50	55.37	6.37	99.93
11	2.57	3.60	8.75	2.40	0.40	0.59	78.65	3.02	99.98
12	1.43	11.91	17.45	4.02	1.72	0.58	58.66	3.11	98.88
13	0.85	3.53	16.78	4.72	2.58	0.58	65.27	4.35	98.66
14	3.73	42.35	14.28	3.73	1.84	0.29	30.11	2.18	98.51
15	1.57	12.40	15.07	2.57	0.54	0.66	62.27	3.89	98.97

Figure 8. SEM images (**a**–**c**) and EDS microanalysis (**d**) of MBIOCl-10 mortar at 28 days.

2.3. Photocatalytic Activity

The R_{NO} for the samples MBiOI-5 and MBiOI-10 under visible light, at the age of 14 days, were 15 and 27%. For MBiOCl-5 and MBiOCl-10 under UV, the values were 23 and 38%, respectively. In both series, the photocatalytic activity was significantly enhanced when the content by mass of photocatalyst was increased from 5 to 10% attributed

to a major availability of photoactive sites on the surfaces of the mortars [44–46]. The addition of BiOX photocatalysts used can be considered high in comparison with the usual dosage of nanoTiO_2-based materials, which normally does not exceed 5% on weight of cement [22,47,48]. However, as previously observed by SEM analysis on 10% BiOX modified-cement samples, its micrometric size allowed suitable dispersion (no agglomeration) of the particles in the cementitious matrix. Furthermore, there was no effect on the compressive mechanical performance (see Figure 5).

Concerning ageing outdoors, Figure 9a,b shows the results for NO removal (bar graphs) and loss of activity (line graphs) every two months, for samples MBiOI and MBiOCl, respectively, in outdoor conditions. During the six first month exposure, the average NO conversion of the MBiOI-5 sample was close to the initial conversion, which was ~15%. After this time, the photocatalytic activity decreased to a value of 1% after 11 months' exposure. In the case of the MBiOI-10 sample, the percentage gradually decreased, resulting in NO conversion of 4% after 11 months of exposure. The NO conversion for MBiOCl samples was stable for the first 4 months, regardless of the load of photocatalyst, even with an increase after intense rain in month 4. After this time, the photocatalytic activity gradually decreased to values of about 2–3% after 11 months.

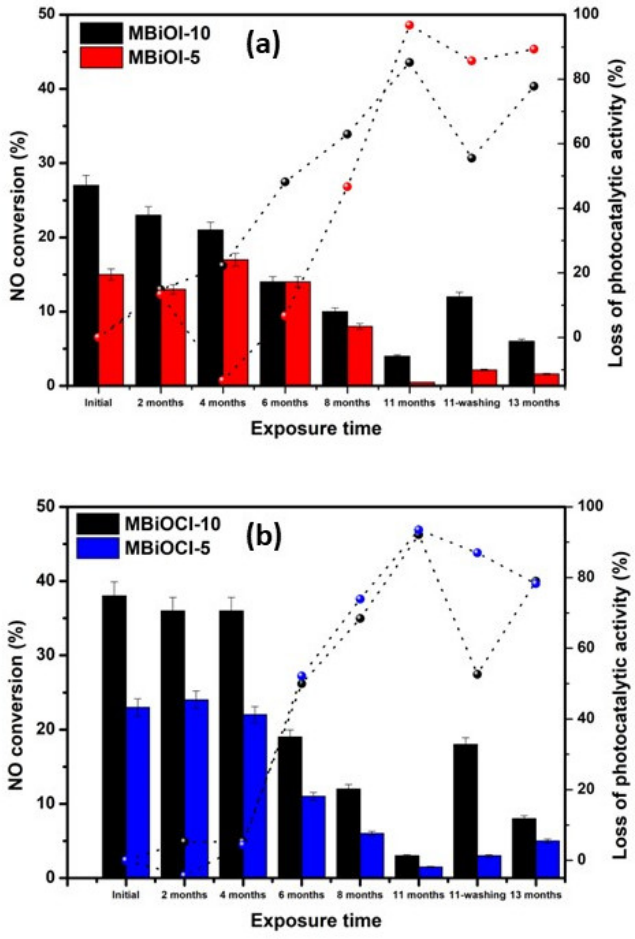

Figure 9. NO removal (bars) and loss of photocatalytic activity (lines) of mortar samples exposed to outdoor weathering during 1-year: (**a**) MBiOI-5 and MBiOI-10 and (**b**) MBiOCl-5 and MBiOCl-10.

The decrease in photocatalytic performance of the samples over time can be associated with natural aging after outdoor exposure, especially due to climatic conditions [49]. Environmental stress may cause coating/binder degradation, particle releases and consequent detachments [50]. Furthermore, partial deactivation due to dirt accumulation, adsorption of pollutants, or reaction by-products (nitrate/nitrite ions accumulation) from NO_x air

oxidation being on the surface might occur in outdoor exposure conditions. Adsorbed NO_3^- can also block catalytic sites from further NO/NO_2 adsorption, and reduction back to NO_2 is likely, reducing nitrate selectivity [51].

Regeneration of the photocatalytic activity due to surface dirtying and poisoning can be achieved by water cleaning of the surfaces [52]. Water flow (or rain) can improve the photocatalytic activity by removing the adsorbed species if they are not strongly adhered. This can explain the behavior of the samples after 4 months of exposure, which coincided with a high level of precipitation (see Figure 10).

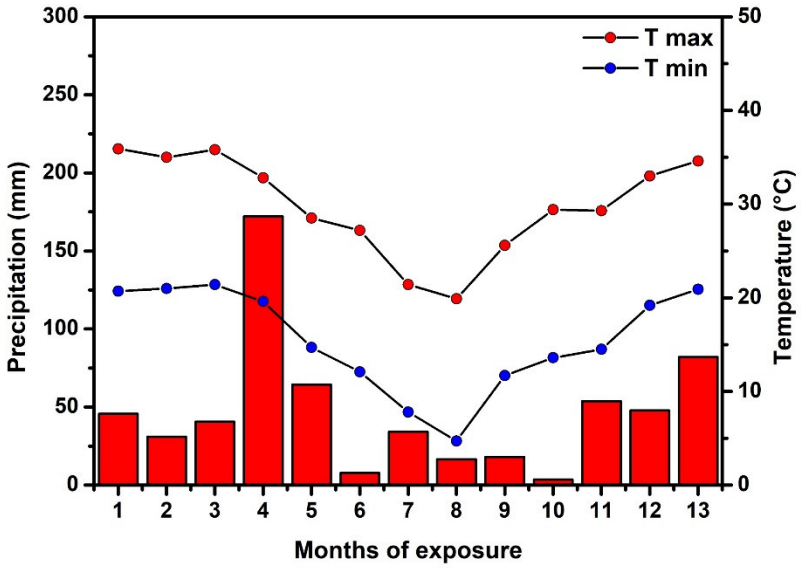

Figure 10. Averaged environmental temperatures and amount of rain during the months of outdoor exposure.

To assess the effect of cleaning the photocatalytic surfaces, BiOX samples were washed with deionized water after 11 months of continuous weathering exposure. Prior to water cleaning, the samples were pre-treated with sandpaper (grade 60) using moderate pressure to remove dirt. After that, the samples were tested for NO removal, and then exposed to the outdoor for another two months. Figure 9 shows the performances of the photocatalytic materials before and after washing. All the samples recovered some activity. The samples containing 10% photocatalyst, MBiOI-10 and MBiOCl-10, achieved values of 44% and 47% of their initial performances, respectively. The cleaning effect was less noticeable in the 5% samples, which only reached ~14% of its starting value. This could have been because the samples with higher BiOX content, which had higher photocatalytic NO conversion yields, accumulated more soluble nitrates on the surfaces that were limiting the real effectiveness of the samples.

Besides that, the loss of photocatalytic activity in cement-based materials can be also attributed to the accumulation of calcium carbonates (calcite, $CaCO_3$) due to the natural carbonation process. The physico-chemical process of carbonation consists of the reaction of atmospheric carbon dioxide (CO_2) with portlandite ($Ca(OH)_2$) or other calcium-bearing phases, (C-S-H) and water to form calcium carbonate ($CaCO_3$, calcite) in Portland cement paste [53]. In general, the microstructure of cement-based materials becomes denser as the carbonation process progresses due to calcium carbonates tending to accumulate on the pores of cementitious materials. As a result, some photocatalyst particles exposed on the surfaces of the cement-based materials may be partially blocked, resulting in a smaller number of active sites being available to react with the pollutants, potentially lowering photocatalytic efficiency [54].

Figure 11 shows the results of carbonation degree after the 13 months of outdoor exposure, after applying the phenolphthalein spray. This solution appears pink in contact

with alkaline concrete with pH values in excess of 9, and colorless at lower levels of pH. When the solution changes to colorless, the cement mixture can be considered carbonated. The surface and depth of carbonation (transversal cut) of mortar samples were assessed. A visual examination confirmed that after been sprayed with phenolphthalein indicator, all of the photoactive surfaces of the mortars remained colorless, indicating that the photoactive surfaces were completely carbonated. As the percentage of photocatalyst increased from 5 to 10%, the pink section on the transverse section of each sample was gradually reduced. Thus, MBiOI-10 and MBiOCl-10 samples had maximum carbonation depth. The increase in carbonation depth of high photocatalyst–containing mortars has been attributed to a decrease in alkaline reserves caused by a decrease in cement content in the samples, together with an increase in porosity, as demonstrated in [42].

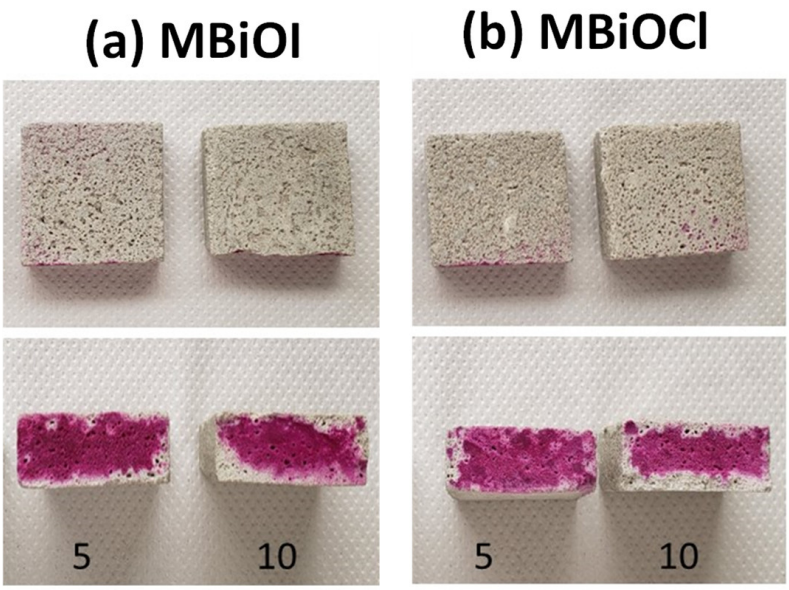

Figure 11. Carbonation test according to the phenolphthalein indicator of photocatalytic mortars with different contents of BiOX (5 and 10%) exposed to real weathering for 13 months.

Additional NO_x air purification tests on the samples were performed to further investigate the effect of carbonation. Figure 12 shows the NO and NO_2 concentration profiles of photocatalytic tests performed 4 years after the outdoor exposure tests were completed for BiOCl and BiOI with 5 and 10% of photocatalyst, respectively. The tests were carried out under ISO standard conditions on the external carbonated surfaces and on a fresh internal surfaces (parallel cut to the external surface). The other non-carbonated surface section was tested under the conditions of the initial tests during the outdoor exposure (1 L/min NO in dry gas). The percentages of NO ($R_{NO}{}^{-}$) and NO_x removal ($R_{NOx}{}^{-}$), and selectivity to nitrates, $S_{NO3-,}$ are also included in the table in Figure 12.

Figure 12 shows that the performance of the BiOI samples continued to deteriorate after four years of storage in plastic wrap protected from external aggression. BiOCl mortar samples presented similar activity after 5 years (having been exposed to outdoor conditions for 13 months), whereas BiOI-5 completely lost it, and BiOI-10 had very low efficiency. Furthermore, there were no discernible differences in activity between carbonated and freshly internal surfaces (non-carbonated) in the ISO standard tests. Aside from that, the fresh surfaces were not exposed to dirt or nitrate accumulation. This suggests that in addition to the surface's deactivation caused by these factors (carbonation and dirt accumulation), a self-deactivation process of the photocatalyst may have occurred in the BiOI samples. As a hypothesis, it could have been due to changes in the phases of the photocatalyst due to the highly alkaline pH, as already pointed out in [42], or evolution processes in the bulk of the cement material.

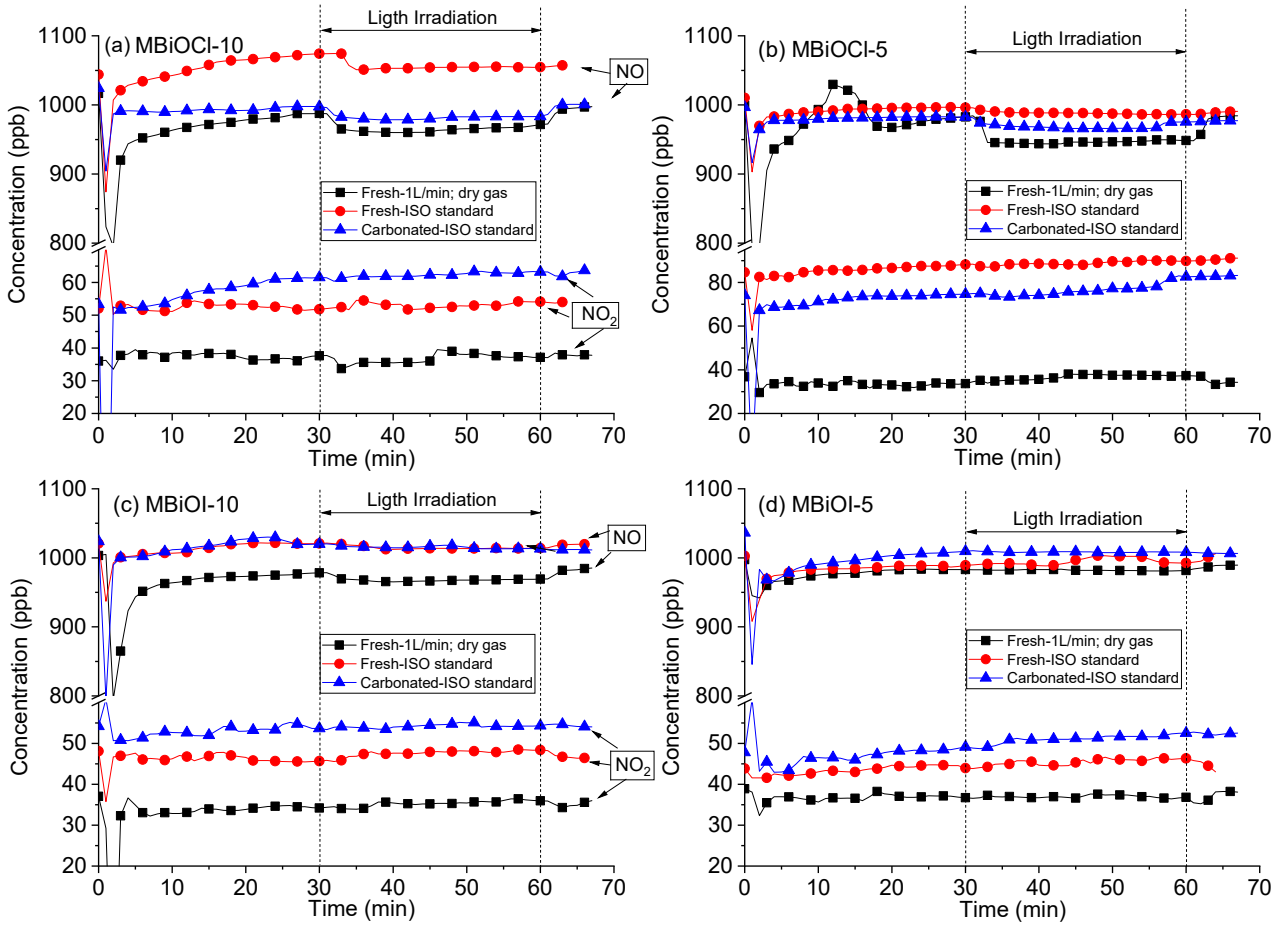

	R_{NO}		R_{NOX}		SNO_3^-		R_{NO}		R_{NOX}		SNO_3^-	
	% BiOCl						% BiOI					
Sample-test conditions	**5%**	**10%**	**5%**	**10%**	**5%**	**10%**	**5%**	**10%**	**5%**	**10%**	**5%**	**10%**
Fresh-ISO test	1.69	3.59	1.45	3.19	0.86	0.89	0	1.28	0	0.84	-	0.65
Carbonated-ISO test	2.95	3.39	2.42	3.04	0.82	0.90	0.20	0.9	0	0.81	-	0.83
Fresh-1L/min dry gas	7.48	4.85	6.61	4.85	0.88	0.99	0.18	2.24	0.12	1.93	0.66	0.86

Figure 12. NO and NO_2 concentration profiles during the photocatalytic tests for BiOCl and BiOI with 5 and 10% of photocatalyst. The percentages of removed NO (R_{NO}) and NO_x (R_{NOx}), and selectivity to nitrates, S_{NO3}^-, are given below.

3. Materials and Methods

3.1. Synthesis of BiOX (X = I and Cl)

Bismuth oxyiodide (BiOI) and bismuth oxychloride (BiOCl) were synthesized according to the procedures described in our previous work [36]. BiOI was prepared by microwave-assisted solvothermal synthesis. In a typical synthesis, 1 mmol de bismuth nitrate pentahydrate ($Bi(NO_3)_3{\cdot}5H_2O$) and potassium iodide (KI) were dissolved in 10 mL ethylene glycol, separately. The KI solution was added by dropping it into a $Bi(NO_3)_3{\cdot}5H_2O$ solution. The resulting solution was kept stirring for another 5 min and heated in a microwave reactor (Monowave 300 Anton Par from 25 to 125 °C using 800 W microwave irradiation), and the reaction proceeded at 125° for 15 min. The product was cooled to room temperature, centrifuged, washed and air-dried at 70 °C for 24 h. BiOCl was prepared by co-precipitation synthesis. Firstly, a 0.1 M solution of $Bi(NO_3)_3{\cdot}5H_2O$ in acetic acid (9% V/V) was prepared. Solutions 0.1 M of ethylenediaminetetraacetic acid disodium salt

dihydrate (EDTA) and potassium chloride (KCl) dissolved in deionized water were also prepared. Then, 40 mL of EDTA solution and 100 mL $Bi(NO_3)_3 \cdot 5H_2O$ solution were mixed by dropping. After 30 min under continuous stirring, 60 mL of a KCl solution was added drop by drop. The resulting product was cooled at room temperature for 24 h, washed by centrifugation to remove reaction by-products and air-dried at 70 °C for 24 h.

3.2. Preparation of Photocatalytic Cement-Based Materials

Two mortar sets were prepared by replacing the 5% and 10% of the weight of cement (Portland cement 40R) with each photocatalyst (BiOCl and BiOI). Reference mortar without photocatalyst, named M-Ref, was also cast. Photocatalytic mortars were labeled MXX-p, where XX represents the type of photocatalyst and p is the percentage added. To achieve a homogeneous solution, the photocatalyst was firstly dispersed in distilled water and sonicated in an ultrasound bath (Bransonic, 1510R-MT) for 5 min. Subsequently, the cement and aqueous dispersion was blended in a mixing pot at a water/cement ratio of 0.485 before gradually adding silica sand to the mixture. The mortars that resulted were cast into wood molds with internal dimensions of 100 mm × 50 mm × 5 mm. After the casting process, the specimens were wrapped with plastic film to prevent moisture evaporation and were kept in the molds for 24 h. Finally, the samples were demolded and submerged in water at 25 ± 3 °C until reaching 28 days in age.

3.3. Characterization of the Photocatalysts

A detailed analysis of the physicochemical and optical properties of the BiOX powders is given in [42]. A summary of the main physicochemical properties of BiOX samples (BiOI and BiOCl) is shown in Table 1. For comparison purposes, the characteristics of commercial Aeroxide®® TiO_2 P25 (Evonik) are also included. The crystalline sizes of BiOX using the Scherrer equation were 8 ± 3 and 12 ± 4 nm for BiOI and BiOCl, respectively; both smaller than TiO_2 (35 nm). The band gap (eV) was calculated by Equation (1) based on diffuse reflectance [55].

$$\alpha hv = A(hv - Eg)^{n/2} \quad (1)$$

where α, h, v, Eg and A are absorption coefficient, Plank constant, light frequency, band gap energy and a constant, respectively. Among them, n is determined by a semiconductor's type of optical transition (n = 1 for direct transition and n = 4 for indirect transition). For BiOx, the value of n is 4 [42]. As a result, the Eg of photocatalyst samples were calculated from a plot of $(hv)^{1/2}$ versus energy (hv) and are summarized in Table 1. BiOCl and TiO_2 samples had similar band gaps of 3.4 and 3.2 eV, respectively, whereas BiOI samples had a smaller one (1.9 eV). This means that TiO_2 and BiOCl samples are active when exposed to UV light, whereas BiOI is active in the visible light range provided by solar irradiation. In terms of specific BET area, BiOI has a greater surface area (57 $m^2\ g^{-1}$) than the reference TiO_2 photocatalyst (50 $m^2\ g^{-1}$) and BiOCl (40 $m^2\ g^{-1}$), which has been found to play a significant role in heterogeneous reactions between solids and gases [26].

The elemental composition and chemical states were analyzed by X-ray photoelectron spectroscopy (XPS) using a Thermo Scientific K-alpha X-ray photoelectron spectrometer system (Waltham, MA, USA) with monochromatized Al Kα radiation (1486.6 eV). The C 1s signal at 284.8 eV was used as a reference. In addition, the morphology and microstructure of the samples were determined using scanning electron microscopy (SEM, Hitachi S-4800, Tokyo, Japan) and transmission electron microscopy (TEM, FEI-Titan G2 80-300, Portland, OR, USA).

3.4. Characterization of Photocatalytic Mortars

The impact of BiOX's addition was studied by comparing the reference mortar without a photocatalyst (MRef) with mortar samples prepared with 10% photocatalyst after 28 days. The hydration process of the mortars was stopped for this propose by immersing them completely in isopropanol for seven days. Compressive strength tests were performed on 50 mm cube specimens using an Instrom universal testing machine by applying a

90 kg/s loading rate. X-ray diffraction patterns (XRD) of powder mortars were obtained by a Bruker D8 Advance diffractometer (Billerica, MA, USA) using Cu Kα radiation at 40 kV and 30 mA. The Hitachi S-4800 microscope (Tokyo, Japan) at 25 Kv was used for the SEM-EDS analysis.

3.5. Exposure of Photocatalytic Mortars to Real Weathering

The photocatalytic performance durability of modified BiOX/cement samples was assessed as a function of time exposed to real-world weathering conditions. From June 2017 to July 2018, the samples (MBiOX with 5 and 10% wt.) remained outdoors. To maximize exposure to sunlight, samples were placed on the roof of an institutional building in the northwest direction (Nuevo Leon, Mexico, 25.7645°, 100.1239°) [13]. Figure 10 depicts the monthly averaged maximum and minimum temperatures, and the amount of rain, during the months of outdoor exposure. The samples were analyzed in the laboratory every two months for NO removal activity in a continuous flow reactor. The reactor was made of stainless steel, and the size of the samples was 100 mm × 50 mm × 5 mm, leaving a 5 mm space in the upper part for gas flow. The target NO gas at a concentration of 3 ppm (N_2 balance) was diluted to 1 ppm by air introduced by a zero-air generator (Environics 6100), and the flow rate of gas was adjusted to 1 L min^{-1}. In the reactor, the content of water vapor was <0.4 ppm, and the temperature was 25 °C ± 2 °C. These conditions are preferable to ISO 22197-1:2007 prescriptions for removal of NO_x, allowing obtaining high sensitivity to activity loss due to weathering. The NO_x stream flowed over the sample in the dark in order to stabilize the adsorption–desorption equilibrium. After this, the mortar samples were illuminated for 30 min. For MBiOI mortars, an LED lamp emitting between 400 and 700 nm (Street Light, DELIGHT, MidView, Singapore, SPL-24 W) was used. MBiOCl samples were irradiated by two UV lamps emitting mainly at 365 nm (TecnoLite, Zapopan, Mexico, 20 W). The obtained results were expressed as percentages of NO and NO_x removed, R_{NO} % and R_{NOx} %, respectively, and NO_2 formed. The nitrate selectivity was expressed as S_{NO3} and calculated as R_{NOx}/R_{NO} [51,56].

The impact of carbonation caused by atmospheric CO_2 on the loss of photocatalytic activity of BiOX/cement samples was assessed after outdoor exposure using phenolphthalein indicator solution at 1% in isopropanol. Following carbonation analysis, the samples were plastic wrapped and stored in a desiccator for 4 more years at room temperature, shielded from the outside environment. Following this period, the NO_x activity of the 5% and 10% specimens was re-examined. After cutting each specimen parallel to the external surface, the analysis was performed on both the outer (carbonated) and inner surfaces of the specimens (freshly internal surface). These tests were carried out in the same conditions as the previous ones (1 L/min NO in dry gas) and in the ISO conditions (3 L/min, 50% RH, 10 W/m^2). The emission spectra of the lamps used for these NO_x photodegradation tests (UV-Visible for BiOCl and Visible for BiOI) are shown in Figure 13. NO_x concentrations were monitored by a chemiluminescent NO_x analyzer.

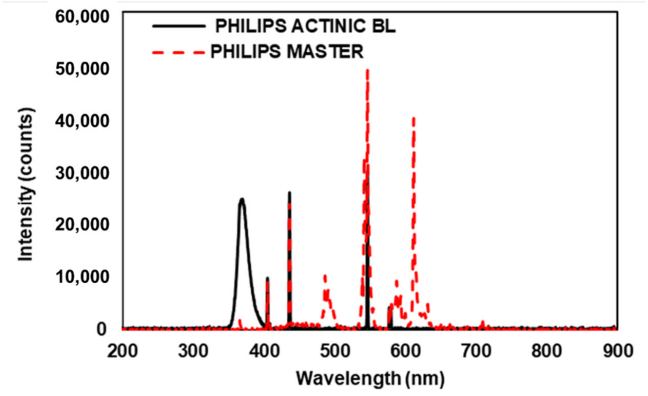

Figure 13. Light spectra for visible (Philips master) and UV-Visible (Philips actinic BL) lamps.

4. Conclusions

A study of photocatalytic BiOX (X = Cl, I) at different percentages (5 and 10% by weight of the cement binder) was carried out outdoors for 13 months, in a temperate context in Nuevo Leon (Mexico), and for 4 additional years in a consistent laboratory environment. The following conclusions have been obtained:

The proposed optimum dosage of BiOX for cement-based materials is 10%, based on results from both compressive mechanical performance and initial photocatalytic performance (NO removal efficiency).

The NO monitoring showed that, after natural weather exposure, a significant decrease in the photoactivity of BiOX mortar samples occurred, leading to values around a 3% of initial performance. Partial regeneration of the photocatalytic activity could be observed after cleaning of the samples, more so in samples with the higher photocatalyst load, indicating that loss of outdoor activity is partially due to external agents, such as dirt and deposition of nitrates.

After four years of subsequent storage, protected from external aggressions in plastic wrap, the mortars with BiOI almost completely lost their activity, whereas BiOCl-10 maintained around 3% RNO_x according the ISO standard conditions, which is similar to the values found after the outdoor period. Carbonation did not seem to be the cause of the decrease in activity, as there were not noticeable differences in NO_x removal activity between carbonated and non-carbonated surfaces. An internal self-deactivation mechanism affecting BiOI photocatalysts in cementitious matrices has been postulated.

Author Contributions: Conceptualization, M.C. and A.M.-d.l.C.; methodology, M.Y.N.-N. and E.J.-R.; validation, M.C., A.M.-d.l.C. and E.J.-R.; formal analysis, M.Y.N.-N.; investigation, E.J-R. and M.Y.N.-N.; resources, A.M.-d.l.C. and M.C.; data curation, E.J.-R.; writing—original draft preparation, M.Y.N.-N.; supervision, M.C.; All authors have read and agreed to the published version of the manuscript.

Funding: This research received no external funding.

Data Availability Statement: Not applicable.

Acknowledgments: The authors are grateful to Maria Grande and Jorge Ruiz for their help in the experimental part.

Conflicts of Interest: The authors declare no conflict of interest.

References

1. Fujishima, A.; Zhang, X.; Tryk, D.A. Heterogeneous photocatalysis: From water photolysis to applications in environmental cleanup. *Int. J. Hydrog. Energy* **2007**, *32*, 2664–2672. [CrossRef]
2. Bengtsson, N.; Castellote, M. Photocatalytic Activity for NO Degradation by Construction Materials: Parametric Study and Multivariable. *Correlations. J. Adv. Oxid. Technol.* **2010**, *13*, 341–349.
3. Laplaza, A.; Jiménez-Relinque, E.; Campos, J.; Castellote, M. Photocatalytic behavior of colored mortars containing TiO_2 and iron oxide based pigments. *Constr. Build Mater.* **2017**, *144*, 300–310. [CrossRef]
4. Calvo, J.G.; Carballosa, P.; Castillo, A.; Revuelta, D.; Gutiérrez, J.; Castellote, M. Expansive concretes with photocatalytic activity for pavements: Enhanced performance and modifications of the expansive hydrates composition. *Constr. Build. Mater.* **2019**, *218*, 394–403. [CrossRef]
5. Diamanti, M.; Del Curto, B.; Ormellese, M.; Pedeferri, M. Photocatalytic and self-cleaning activity of colored mortars containing TiO_2. *Constr. Build. Mater.* **2013**, *46*, 167–174. [CrossRef]
6. Farzadnia, N.; Ali, A.A.A.; Demirboga, R.; Anwar, M.P. Characterization of high strength mortars with nano Titania at elevated temperatures. *Constr. Build. Mater.* **2013**, *43*, 469–479. [CrossRef]
7. Jimenez-Relinque, E.; Castellote, M. Rapid assessment of the photocatalytic activity in construction materials: Pros and cons of reductive inks and oxidative fluorescence probes versus standardized NO_x testing. *Catal. Today* **2019**, *358*, 164–171. [CrossRef]
8. Macphee, D.E.; Folli, A. Photocatalytic concretes—The interface between photocatalysis and cement chemistry. *Cem. Concr. Res.* **2016**, *85*, 48–54. [CrossRef]
9. Folli, A.; Strøm, M.; Madsen, T.P.; Henriksen, T.; Lang, J.; Emenius, J.; Klevebrant, T.; Nilsson, Å. Field study of air purifying paving elements containing TiO_2. *Atmos. Environ.* **2015**, *107*, 44–51. [CrossRef]

10. Jiménez-Relinque, E.; Hingorani, R.; Rubiano, F.; Grande, M.; Castillo, Á.; Castellote, M. In situ evaluation of the NO_x removal efficiency of photocatalytic pavements: Statistical analysis of the relevance of exposure time and environmental variables. *Environ. Sci. Pollut. Res.* **2019**, *26*, 36088–36095. [CrossRef]
11. Ballari, M.M.; Brouwers, H.J.H. Full scale demonstration of air-purifying pavement. *J. Hazard. Mater.* **2013**, *254–255*, 406–414. [CrossRef]
12. Guerrini, G.L.; Crespo, R.; Jurado, R. Use of photocatalytic cements on urban roads with high traffic volumes. *Carreteras* **2017**, *4*, 49–55.
13. Cordero, J.; Hingorani, R.; Jiménez-Relinque, E.; Grande, M.; Borge, R.; Narros, A.; Castellote, M. NO_x removal efficiency of urban photocatalytic pavements at pilot scale. *Sci. Total Environ.* **2020**, *719*, 137459. [CrossRef] [PubMed]
14. Jimenez-Relinque, E.; Castellote, M. Influence of the inlet air in efficiency of photocatalytic devices for mineralization of VOCs in air-conditioning installations. *Environ. Sci. Pollut. Res.* **2014**, *21*, 11198–11207. [CrossRef]
15. Auvinen, J.; Wirtanen, L. The influence of photocatalytic interior paints on indoor air quality. *Atmos. Environ.* **2008**, *42*, 4101–4112. [CrossRef]
16. Ai, Z.; Ho, W.; Lee, S.; Zhang, L.J.E.s. Efficient photocatalytic removal of NO in indoor air with hierarchical bismuth oxybromide nanoplate microspheres under visible light. *Environ. Sci. Technol.* **2009**, *43*, 4143–4150. [CrossRef] [PubMed]
17. Mo, J.; Zhang, Y.; Xu, Q.; Lamson, J.J.; Zhao, R. Photocatalytic purification of volatile organic compounds in indoor air: A literature review. *Atmos. Environ.* **2009**, *43*, 2229–2246. [CrossRef]
18. European Environmental Agency (EEA). Report, no. 15/2021. Air quality in Europe 2021. Available online: https://www.eea.europa.eu/publications/air-quality-in-europe-2021 (accessed on 1 June 2022).
19. Chen, J.; Kou, S.-c.; Poon, C.-s. Photocatalytic cement-based materials: Comparison of nitrogen oxides and toluene removal potentials and evaluation of self-cleaning performance. *Build. Environ.* **2011**, *46*, 1827–1833. [CrossRef]
20. Cassar, L. Photocatalysis of cementitious materials: Clean buildings and clean air. *MRS Bull.* **2004**, *29*, 328–331. [CrossRef]
21. Folli, A.; Pade, C.; Hansen, T.B.; De Marco, T.; Macphee, D.E. TiO_2 photocatalysis in cementitious systems: Insights into self-cleaning and depollution chemistry. *Cem. Concr. Res.* **2012**, *42*, 539–548. [CrossRef]
22. Jimenez-Relinque, E.; Rodriguez-Garcia, J.; Castillo, A.; Castellote, M. Characteristics and efficiency of photocatalytic cementitious materials: Type of binder, roughness and microstructure. *Cem. Concr. Res.* **2015**, *71*, 124–131. [CrossRef]
23. Enea, D.; Guerrini, G.L. Photocatalytic properties of cement-based plasters and paints containing mineral pigments. *Transp. Res. Rec.* **2010**, 52–60. [CrossRef]
24. Maggos, T.; Bartzis, J.; Liakou, M.; Gobin, C. Photocatalytic degradation of NO_x gases using TiO_2-containing paint: A real scale study. *J. Hazard. Mater.* **2007**, *146*, 668–673. [CrossRef]
25. Mills, A.; O'Rourke, C.; Lawrie, K.; Elouali, S. Assessment of the Activity of Photocatalytic Paint Using a Simple Smart Ink Designed for High Activity Surfaces. *ACS Appl. Mater. Interfaces* **2014**, *6*, 545–552. [CrossRef]
26. Luévano-Hipólito, E.; Martínez-De La Cruz, A. Photocatalytic stucco for NO_x removal under artificial and by real weatherism. *Constr. Build. Mater.* **2018**, *174*, 302–309. [CrossRef]
27. da Silva, A.L.; Dondi, M.; Raimondo, M.; Hotza, D. Photocatalytic ceramic tiles: Challenges and technological solutions. *J. Eur. Ceram. Soc.* **2018**, *38*, 1002–1017. [CrossRef]
28. Carrillo, H.G.; Relinque, E.J.; Ramírez, A.M.; Castellote, M.; Pérez, M.R. Optimising processing conditions for the functionalisation of photocatalytic glazes by ZnO nanoparticle deposition. *Mater. Construcción* **2021**, *71*, 344.
29. Chengyu, W.; Huamei, S.; Ying, T.; Tongsuo, Y.; Guowu, Z. Properties and morphology of CdS compounded TiO_2 visible-light photocatalytic nanofilms coated on glass surface. *Sep. Purif. Technol.* **2003**, *32*, 357–362. [CrossRef]
30. Hurum, D.C.; Gray, K.A.; Rajh, T.; Thurnauer, M.C. Recombination pathways in the Degussa P25 formulation of TiO_2: Surface versus lattice mechanisms. *J. Phys. Chem. B* **2005**, *109*, 977–980. [CrossRef]
31. Jimenez-Relinque, E.; Castellote, M. Hydroxyl radical and free and shallowly trapped electron generation and electron/hole recombination rates in TiO_2 photocatalysis using different combinations of anatase and rutile. *Appl. Catal. A Gen.* **2018**, *565*, 20–25. [CrossRef]
32. Landsberg, P.T. Recombination in Semiconductors 1991, 600. Available online: https://onlinelibrary.wiley.com/doi/abs/10.1002/adma.19930050123 (accessed on 1 June 2022).
33. David Dankovic, E.K.; Geraci, C.; Gilbert, S.; Rice, F.; Schulte, P.; Smith, R.; Sofge, C.; Wheeler, M.; Zumwalde, R. *Occupational Exposure to Titanium Dioxide*; Department of health and human services, Centers for disease control and prevention, National Institute for Occupational Safety and Health: Cincinnati, OH, USA, 2011; p. 120.
34. Chen, R.; Hu, B.; Liu, Y.; Xu, J.; Yang, G.; Xu, D.; Chen, C. Beyond PM2.5: The role of ultrafine particles on adverse health effects of air pollution. *Biochim. Biophys. Acta BBA Gen. Subj.* **2016**, *1860*, 2844–2855. [CrossRef] [PubMed]
35. European Commission. Commission Delegated Regulation (EU) 2020/217 of 4 October 2019 amending, for the purposes of its adaptation to technical and scientific progress, Regulation (EC) No 1272/2008 of the European Parliament and of the Council on classification, labelling and packaging of substances and mixtures and correcting that Regulation (Text with EEA relevance). 2020. Available online: https://www.legislation.gov.uk/eur/2020/217 (accessed on 1 June 2022).
36. Nava Núñez, M.; Martínez-de la Cruz, A.; López-Cuéllar, E. Preparation of BiOI microspheres in 2-propanol/ethylene glycol by microwave method with high visible-light photocatalytic activity. *Res. Chem. Intermed.* **2019**, *45*, 1475–1492. [CrossRef]

37. Montoya-Zamora, J.; Martinez-De La Cruz, A.; Lopez-Cuellar, E.; González, F.P. BiOBr photocatalyst with high activity for NO_x elimination. *Adv. Powder Technol.* **2020**, *31*, 3618–3627. [CrossRef]
38. Reyna-Cavazos, K.; la Cruz, A.; Longoria Rodríguez, F.; López-Cuellar, E. Synthesis of bismuth oxyiodide (BiOI) by means of microwaves in glycerol with high photocatalytic activity for the elimination of NO_x and SO_2. *Res. Chem. Intermed.* **2020**, *46*, 923–941. [CrossRef]
39. Zhang, M.; Liu, Y.; Li, L.; Gao, H.; Zhang, X. BiOCl nanosheet/$Bi_4Ti_3O_{12}$ nanofiber heterostructures with enhanced photocatalytic activity. *Catal. Commun.* **2015**, *58*, 122–126. [CrossRef]
40. Geng, Z.; Xin, M.; Zhu, X.; Xu, H.; Cheng, X.; Wang, D. A new method for preparing photocatalytic cement-based materials and the investigation on properties and mechanism. *J. Build. Eng.* **2021**, *35*, 102080. [CrossRef]
41. Wang, D.; Hou, P.; Yang, P.; Cheng, X. BiOBr@ SiO_2 flower-like nanospheres chemically-bonded on cement-based materials for photocatalysis. *Appl Surf. Sci* **2018**, *430*, 539–548. [CrossRef]
42. Nava-Núñez, M.Y.; Jimenez-Relinque, E.; Grande, M.; Martínez-de la Cruz, A.; Castellote, M. Photocatalytic BiOX Mortars under Visible Light Irradiation: Compatibility, NO_x Efficiency and Nitrate Selectivity. *Catalysts* **2020**, *10*, 226. [CrossRef]
43. Kaja, A.M.; Brouwers, H.J.H.; Yu, Q.L. NO_x degradation by photocatalytic mortars: The underlying role of the CH and C-S-H carbonation. *Cem. Concr. Res.* **2019**, *125*, 105805. [CrossRef]
44. Yang, L.; Hakki, A.; Wang, F.; Macphee, D.E. Photocatalyst efficiencies in concrete technology: The effect of photocatalyst placement. *Appl. Catal. B Environ.* **2018**, *222*, 200–208. [CrossRef]
45. Chen, X.-F.; Kou, S.-C.; Poon, C.S. Rheological behaviour, mechanical performance, and NO_x removal of photocatalytic mortar with combined clay brick sands-based and recycled glass-based nano-TiO_2 composite photocatalysts. *Constr. Build. Mater.* **2020**, *240*, 117698. [CrossRef]
46. Yang, L.; Hakki, A.; Zheng, L.; Jones, M.R.; Wang, F.; Macphee, D.E. Photocatalytic concrete for NO_x abatement: Supported TiO_2 efficiencies and impacts. *Cem. Concr. Res.* **2019**, *116*, 57–64. [CrossRef]
47. He, R.; Huang, X.; Zhang, J.; Geng, Y.; Guo, H. Preparation and evaluation of exhaust-purifying cement concrete employing titanium dioxide. *Materials* **2019**, *12*, 2182. [CrossRef]
48. Xu, M.; Clack, H.; Xia, T.; Bao, Y.; Wu, K.; Shi, H.; Li, V. Effect of TiO_2 and fly ash on photocatalytic NO_x abatement of engineered cementitious composites. *Constr. Build. Mater.* **2020**, *236*, 117559. [CrossRef]
49. Guo, M.-Z.; Maury-Ramirez, A.; Poon, C.S. Photocatalytic activities of titanium dioxide incorporated architectural mortars: Effects of weathering and activation light. *Build. Environ.* **2015**, *94*, 395–402. [CrossRef]
50. Jimenez-Relinque, E.; Grande, M.; Duran, T.; Castillo, Á.; Castellote, M. Environmental impact of nano-functionalized construction materials: Leaching of titanium and nitrates from photocatalytic pavements under outdoor conditions. *Sci. Total Environ.* **2020**, 140817. [CrossRef] [PubMed]
51. Bloh, J.Z.; Folli, A.; Macphee, D.E.J.R.A. Photocatalytic NO_x abatement: Why the selectivity matters. *RSC Adv.* **2014**, *4*, 45726–45734. [CrossRef]
52. Dantas, S.R.A.; Vittorino, F.; Loh, K. Photocatalytic performance of white cement mortars exposed in urban atmosphere. *Glob. J. Res. Eng.* **2019**, *19*, 2.
53. Castellote, M.; Andrade, C.; Turrillas, X.; Campo, J.; Cuello, G. Accelerated carbonation of cement pastes in situ monitored by neutron diffraction. *Cem. Concr. Res.* **2008**, *38*, 1365–1373. [CrossRef]
54. Hingorani, R.; Jimenez-Relinque, E.; Grande, M.; Castillo, A.; Nevshupa, R.; Castellote, M. From analysis to decision: Revision of a multifactorial model for the in situ assessment of NO_x abatement effectiveness of photocatalytic pavements. *Chem. Eng. J.* **2020**, *402*, 126250. [CrossRef]
55. Anderson, C.; Bard, A.J. Improved photocatalytic activity and characterization of mixed TiO_2/SiO_2 and TiO_2/Al_2O_3 materials. *J. Phys. Chem. B* **1997**, *101*, 2611–2616. [CrossRef]
56. Jimenez-Relinque, E.; Rubiano, F.; Hingorani, R.; Grande, M.; Castillo, A.; Nevshupa, R.; Castellote, M. New Holistic Conceptual Framework for the Assessment of the Performance of Photocatalytic Pavement. *Front. Chem.* **2020**, *8*, 743. [CrossRef]